Supporting Information

Correlating the Morphological Evolution of Individual Catalyst Particles to the Kinetic Behavior of Metallocene-Based Ethylene Polymerization Catalysts

Maximilian J. Werny,[a,d,‡] Jelena Zarupski,[b,d,‡] Iris C. ten Have,[a] Alessandro Piovano,[b,d] Coen Hendriksen,[c] Nicolaas H. Friederichs,[c] Florian Meirer,[a,d,*] Elena Groppo,[b,d,*] and Bert M. Weckhuysen[a,d,*]

[a] Inorganic Chemistry and Catalysis group, Debye Institute for Nanomaterials Science, Utrecht University, Universiteitsweg 99, 3584 CG Utrecht (The Netherlands)

[b] Department of Chemistry, INSTM and NIS Centre, University of Torino, Via G. Quarello 15A, 10135 Torino (Italy)

[c] SABIC Technology Center, Urmonderbaan 22, 6167 RD Geleen (The Netherlands)

[d] Dutch Polymer Institute (DPI), P.O. Box 902, 5600 AX Eindhoven (The Netherlands)

Table of Contents

Figure S13. For each of the experiments reported in Figure 7 (main text), the maximum intensity of the FT-IR absorption bands T and C was determined by extrapolating the linear part of the curves (indicated as Tn and Cn, where n = 1, 2, 3 refers to the experiments at low, medium and high d-ACN concentration). The insertion rate was derived from the slope of the linear part of the I curves (In, with n = 1, 2 and 3).

References

Experimental Procedures

Section S1: Catalyst preparation

The hafnocene-based (i.e., Hf/MAO/SiO_2) and zirconocene-based (i.e., Zr/MAO/SiO_2) catalyst materials under investigation were provided by SABIC (Saudi Basic Industries Corporation). The catalyst materials were prepared following a two-step procedure. The bis-indenyl metallocene complexes were suspended in dried toluene (Braun solvent purification system) and contacted with methylaluminoxane (MAO, 30 wt%, Chemtura; Al/M molar ratio = 150) as co-catalyst. Then, ES757 silica (PQ Corporation, D_{50} = 25.0 µm, S_{BET} = 295 m^2/g, V_{Pore} = 1.6 mL/g) was added to the solution to form a slurry. The remaining solvent was removed by a stream of N_2 at room temperature for 20 h to produce a free-flowing yellow powder. Prior to impregnation, the ES757 silica was calcined for 4 h at 600 °C. All synthetic procedures were performed under inert N_2 atmosphere. The zirconocene-based and hafnocene-based catalyst materials possess weight loadings of ~ 0.30 wt% Zr and ~ 0.59 wt% Hf, respectively (determined via X-ray fluorescence analysis, XRF).

Section S2: Catalytic testing

Catalytic tests were performed using a medium-throughput testing set-up consisting of 8 parallel reactors (450 mL autoclaves), equipped with helical stirrers, under reaction conditions that are displayed in Table S1.

Due to the technical complexity of conducting gas-phase polymerizations at the lab scale, a methodology described by the group of McKenna,[1–3] involving the addition of NaCl to the reactors, was adopted to ensure a better dispersion of the catalyst as well as improved heat transfer during the polymerization reaction. NaCl sits at the base of the reactors and is stirred by helical stirrers. The catalyst is then added on top and is dispersed throughout the reactor volume.

For a typical gas-phase polymerization experiment, the following procedure was applied. NaCl was dried in an oven at 130 °C for two days prior to transfer to the autoclave. The autoclave was closed and kept at 110 °C while the reactor was flushed 20 times with N_2 to remove impurities. After removal of all impurities, the reactor was conditioned to the required temperature and pressurized to the required C_2H_4 pressure. A slurry of 50 mg catalyst in 2.5 mL pentamethylheptane (PMH) was prepared in the glovebox and the required catalyst amount taken up by a robotic needle. The robotic needle goes through an antechamber to enter the reactor and injects the catalyst slurry using a nitrogen overpressure of 0.5–1.0 bar. Upon injection of the catalyst into the autoclave, the reaction is started. The ethylene pressure is controlled by means of GC analysis of the reactor headspace with an integrated feedback control of the reactor feeds. After 60 min of polymerization, a quench gas was added at overpressure to terminate the reaction. After three venting/vacuum/nitrogen flushing cycles, the reactor was opened.

Table S1. Reaction conditions employed during the high-pressure gas-phase polymerization of ethylene over the hafnocene-based and zirconocene-based catalysts and their respective polyethylene (PE) yields.

Catalyst	Catalyst mass (mg)	C_2H_4 pressure (bar)	Temperature (°C)	Reaction time (min)	Volume TiBA, 3.2 mmol/L (mL)	Stir rate (rpm)	Mass NaCl (g)	Yield (g)
SiO_2/MAO/Hf	12	15	87	60	3.6	600	50	1.8
SiO_2/MAO/Zr	6	15	87	60	3.6	600	50	38

Section S3: Catalyst pre-polymerization

Pre-polymerized samples of the hafnocene-based and zirconocene-based catalysts were prepared under mild conditions via gas-phase ethylene polymerization at 1.6 bar ethylene pressure and room temperature. For this purpose, 6.7 mg of the respective catalyst was added to a dedicated glass-reactor (~ 100 mL, Figure S1) and subjected to constant ethylene pressure for the designated time periods (i.e., 10 min, 30 min and 60 min) using a gas line inside the glovebox. In preparation for each pre-polymerization, the catalyst powder was well dispersed over the glass surface to reduce particle agglomeration and overheating. All gas-phase polymerizations were performed under static conditions (no fluidization). Further information on the set-up can be found in previous work by our group.[4]

Table S2. Polyethylene (PE) yields in g_{PE}/g_{cat} as obtained during the gas-phase polymerization of ethylene over the hafnocene-based and zirconocene-based catalysts in a dedicated glass-reactor set-up (1.6 bar C_2H_4, room temperature).

Catalyst yield (g_{PE}/g_{cat})	10 min	30 min	60 min
SiO_2/MAO/Hf	1.4	2.6	6.7
SiO_2/MAO/Zr	1.4	3.2	5.8

Section S4: Catalyst characterization

A. Focused ion beam - scanning electron microscopy (FIB-SEM) was performed using a FEI Helios NanoLab G3 UC scanning electron microscope following a conventional procedure from literature.[5] All samples were sprinkled onto double-sided adhesive, conductive carbon tape, which was then stuck onto an aluminium SEM stub. A Pt coating of ~ 6 nm was subsequently applied in a Cressington 208HR sputter coater. During the process of FIB cutting, slices were milled perpendicularly or horizontally to the surface using a 45° angled SEM stub at different stage tilt angles. Cross-sectional SEM images were recorded in backscattered electron (BSE) mode using the Through the Lens Detector (TLD) in combination with an immersion lens at 2 kV and 0.1 nA. Image segmentation was performed using the Avizo™ software package by Thermo Fisher Scientific Inc. For images displaying full particle cross-sections, manual thresholds were applied to ensure a correct segmentation of the cross-section into support (light gray), polymer (dark gray) and pore space (predominantly black). Manual adjustments were made to include light gray regions within the pores that correspond to the inner walls of the pore as well as white regions that correspond to Ga and/or Pt deposits from the FIB cutting procedure. This ensured a correct segmentation of the pore space in 2D. Automatic thresholding algorithms falsely segment the pore space as solid phase due to the algorithms' inability to correctly interpret the 3D geometry of the pore system as well as due to Pt and/or Ga deposition in the pores during sputter coating and/or during the FIB cutting procedure (Ga ion beam used for FIB cutting). All close-up images were segmented using Otsu's method.

B. Infrared photoinduced force microscopy (IR PiFM) was performed using a VistaScope photoinduced force microscope (PiFM) from Molecular Vista Inc. (San Jose, CA, USA). The instrument is equipped with a Block Engineering tunable quantum cascade laser (QCL) unit for spectral acquisition in the range of 775–1950 cm^{-1} at 1 cm^{-1} spectral resolution. Atomic force microscopy (AFM) topography images, IR maps and IR point spectra were recorded in dynamic non-contact mode (60 accumulations, 500 ms pixel dwell time, 1 cm^{-1} spectral resolution) using NCHR Au-coated cantilevers (force constant: ~ 40 N/m).

All AFM, IR and phase maps were recorded on the cross-sections of a single 30 min pre-polymerized SiO_2/MAO/Hf particle (Cross-sections 1 and 2; see Figure 2C, Figure 4 and Figure S8). The AFM and IR maps were acquired in non-contact mode at a set point amplitude ratio of 80–85% (i.e., in relation to the free space value). To record phase maps of the corresponding areas, however, the set point was lowered to 60% to enhance tip-sample contact (contact mode), unless specified otherwise. These set point values were chosen based on the shift of the cantilever frequency relative to its eigenfrequency[6] (Table S3), an indicator for the degree of tip-sample interaction. For both the silica and PE phases, set points greater than 60% resulted in a shift to lower frequencies. This implies that net attractive forces are acting on the cantilever tip. The attractive forces were the highest at a set point of 80%. Repulsive tip-sample interactions, on the other hand, start to dominate at a set point of 60% and lead to higher frequencies. Spatial resolutions in the range of 10–40 nm were achieved at a probing depth of approximately 30 nm[7].

Table S3. Cantilever frequency recorded at different amplitude ratio set points on silica- [1030 cm^{-1}, ν(Si–O)] and PE-rich [1472 cm^{-1}, δ(C–H)] domains of a hafnocene-based catalyst particle cross-section (cantilever eigenfrequency: 265.287 kHz, drive amplitude: 3 nm).

Set point	Frequency [1030 cm^{-1}] (kHz)	Frequency [1472 cm^{-1}] (kHz)
90%	264.087	264.087
80%	263.987	263.987
70%	264.787	264.787
60%	265.687	266.787

All data were analysed using the VistaScan 3.9 and SurfaceWorks 3.0 software packages from Molecular Vista Inc. Spectra recorded on the hafnocene-based catalyst particle cross-sections were generally saved without normalization or smoothing. A 2nd-order Savitzky–Golay filter was applied in OriginPro 2016 to decrease the level of background noise. If required, the spectra were also normalized to their highest bands using the same software.

In general, the acquisition of high quality spectral data proved to be challenging for the catalyst particle cross-sections. The polymer phase displayed pronounced sensitivity towards the incident IR laser. As can be seen in Figure S12, its partial degradation is apparent from the emergence of new bands in the IR point spectra. The bands at around 924 cm^{-1} and 1594 cm^{-1} can be linked to δ(C=C–H)[8] and ν(C=C)[8–11] vibrations while the band at 1376 cm^{-1} can be assigned to the vibration of methyl groups[8,10]. These suggest that the scission of the polymer chains has occurred. The band at 1264 cm^{-1} is often associated with the δ(Si–CH_3)[12,13] vibration in polydimethylsiloxane (PDMS), which represents a common contamination on AFM tips. We expect the high degree of intermixing of the silica and PE phases to further impede the acquisition of high quality PE spectra (low local PE concentrations).

C. Fourier transform infrared spectroscopy (FT-IR) in presence of d-acetonitrile as a probe molecule was performed in transmission mode by using a Bruker Vertex70 instrument equipped with a MCT detector at a spectral resolution of 2 cm^{-1}. The samples were measured in the form of thin, self-supporting pellets, made inside the glovebox by using a manual pelletizer. After the pellet was prepared, it was inserted into a gold envelope and placed inside a quartz cell equipped with two KBr windows. In order to monitor the evolution of the spectra in the presence of d-acetonitrile, the quartz cell, interfaced with the spectrophotometer, was directly connected to a vacuum line. Experiments were performed at room temperature at different d-acetonitrile pressures (concentrations). Before dosing d-acetonitrile, the

sample was outgassed in high vacuum for 15 min in order to remove N_2 from the glovebox. During outgassing, small amounts of toluene, used as a solvent during the synthesis, were also removed. After d-acetonitrile was dosed, spectra were collected every 5 min for 3 h.

Supporting Figures

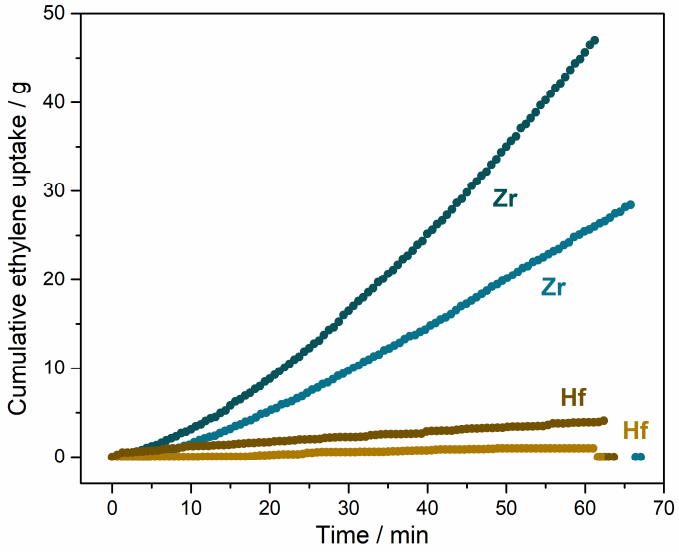

Figure S1. Cumulative ethylene uptake in grams (g) during the high-pressure gas-phase polymerization of ethylene over the hafnocene-based and zirconocene-based catalysts (two runs per catalyst, refer to Section S2 for experimental details).

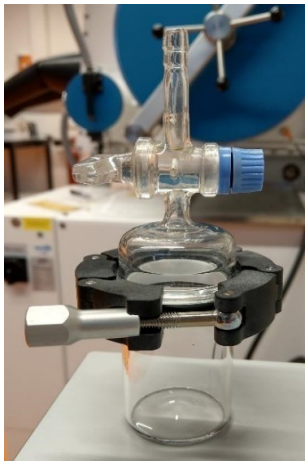

Figure S2. Image of a glass-reactor used in the gas-phase ethylene pre-polymerization of the metallocene-based catalyst materials.

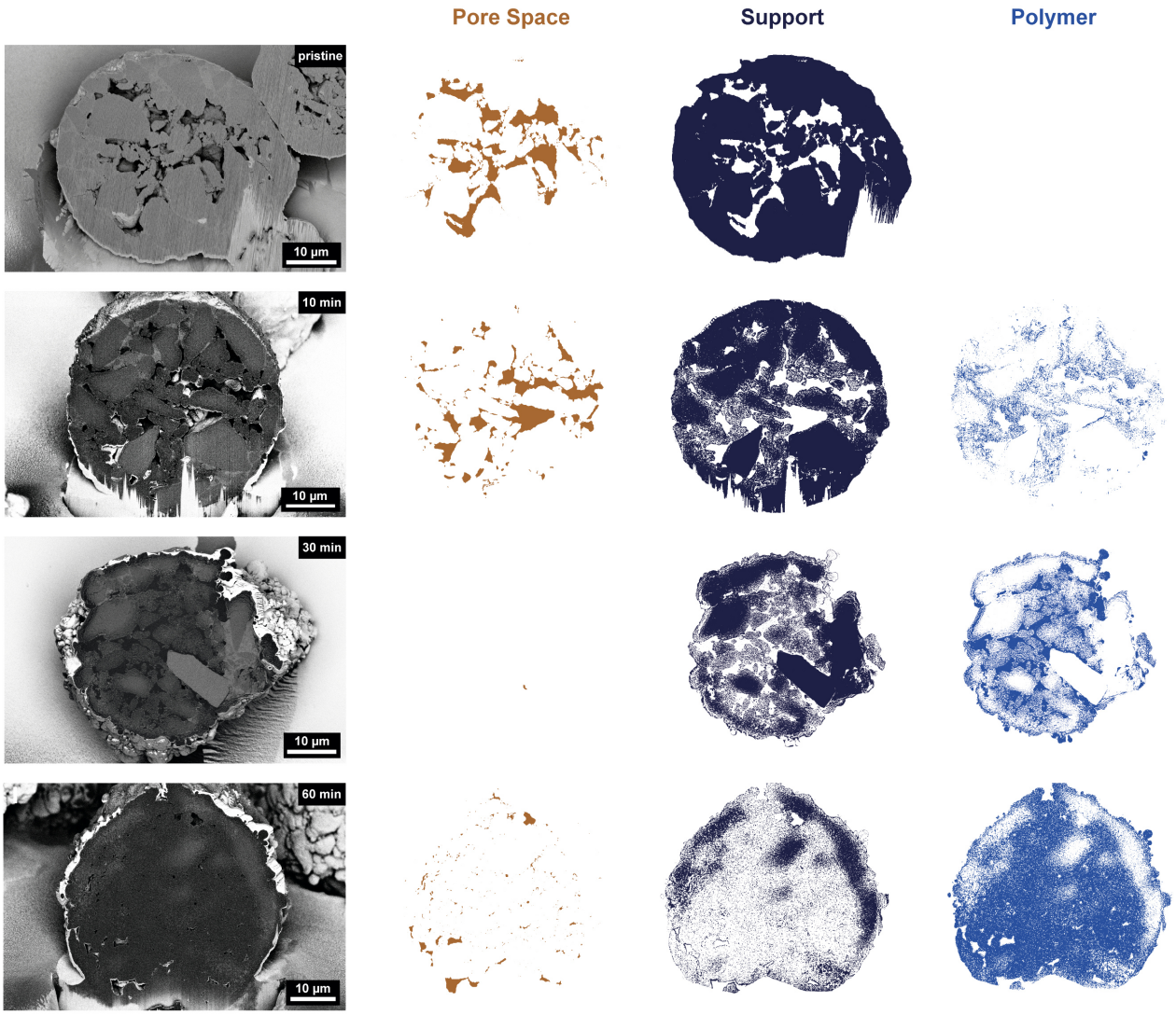

Figure S3. Scanning electron microscopy (SEM) images and corresponding segmentations of the cross-sections of pristine and pre-polymerized hafnocene-based catalyst particles. The pore space, support (silica) and polymer (polyethylene, PE) are illustrated in brown, dark blue and blue, respectively.

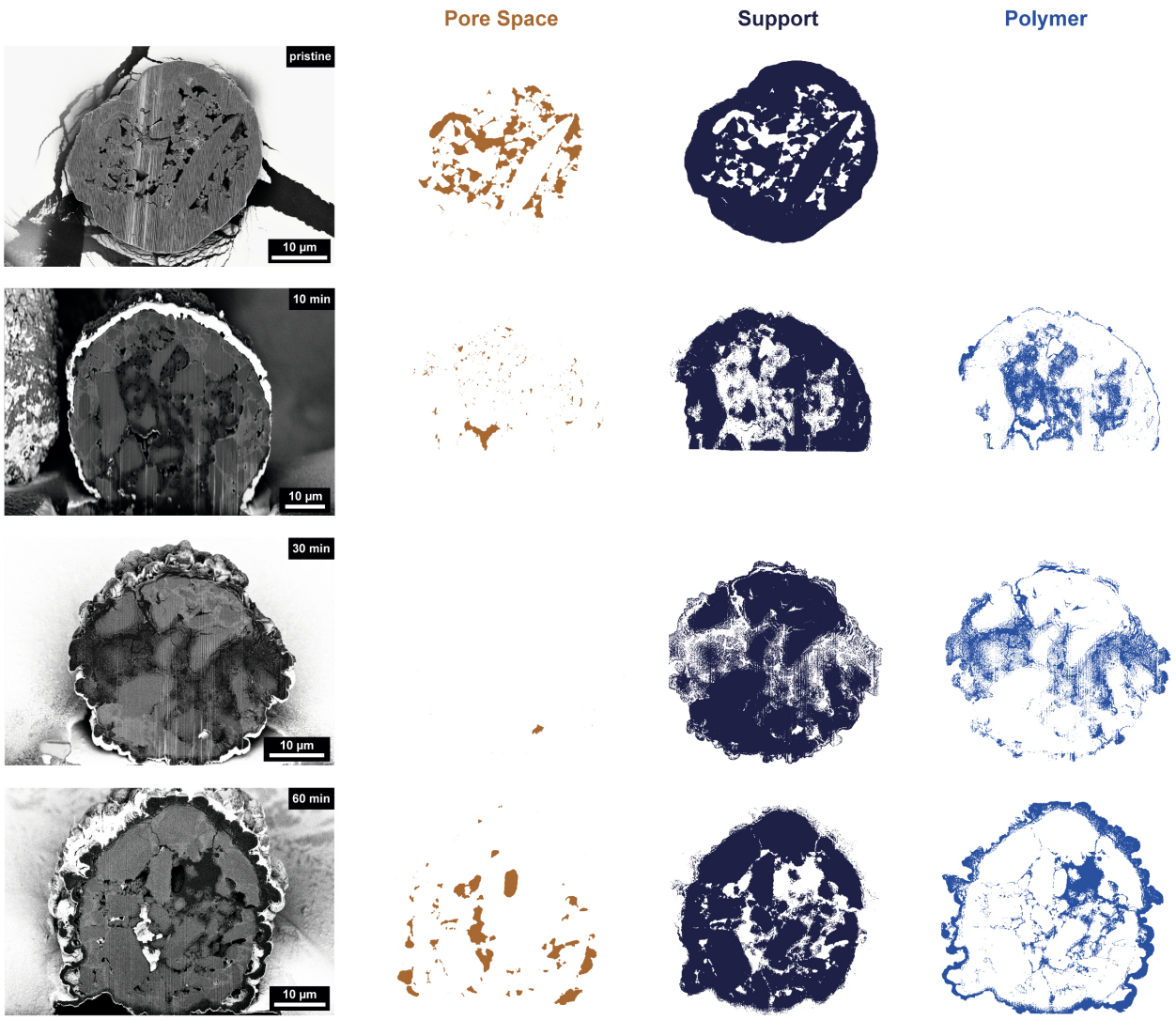

Figure S4. Scanning electron microscopy (SEM) images and corresponding segmentations of the cross-sections of pristine and pre-polymerized zirconocene-based catalyst particles. The pore space, support (silica) and polymer (polyethylene, PE) are illustrated in brown, dark blue and blue, respectively. The lower third of the 10 min pre-polymerized particle was out-of-focus and, thus, excluded from the segmentation.

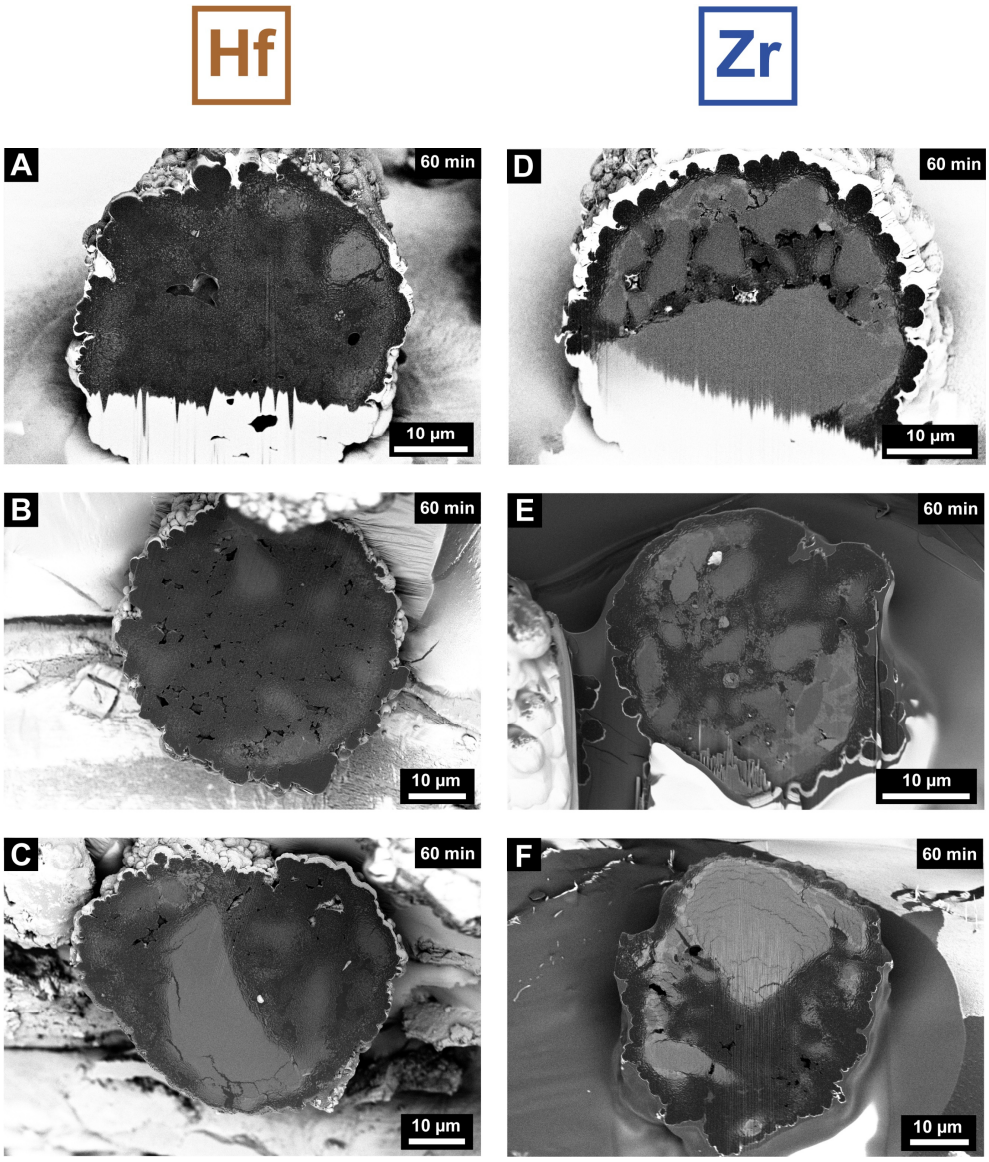

Figure S5. Scanning electron microscopy (SEM) images displaying the cross-sections of 60 min pre-polymerized hafnocene-based (A–C) and zirconocene-based (D–F) catalyst particles (1.6 bar C_2H_4, gas-phase, room temperature).

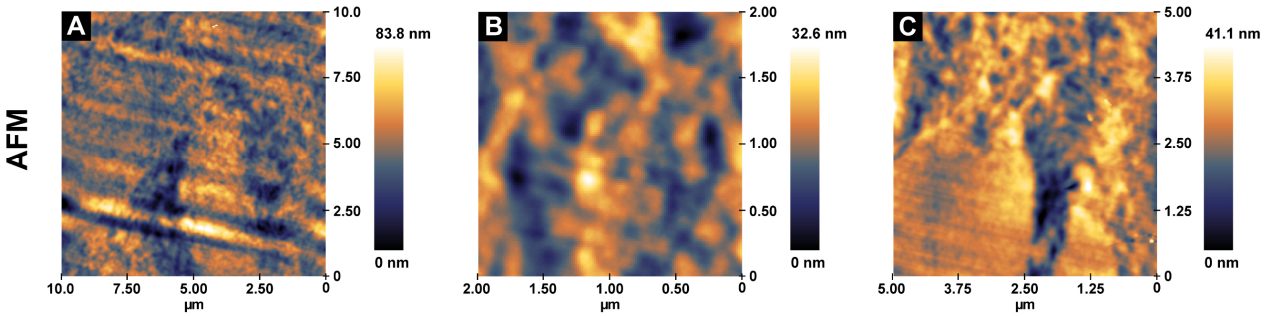

Figure S6. Topography (AFM) maps of three areas of the 30 min pre-polymerized hafnocene-based catalyst particle cross-section that were measured using infrared photoinduced force microscopy (IR PiFM) (Cross-section 1, Figure 4 in main text).

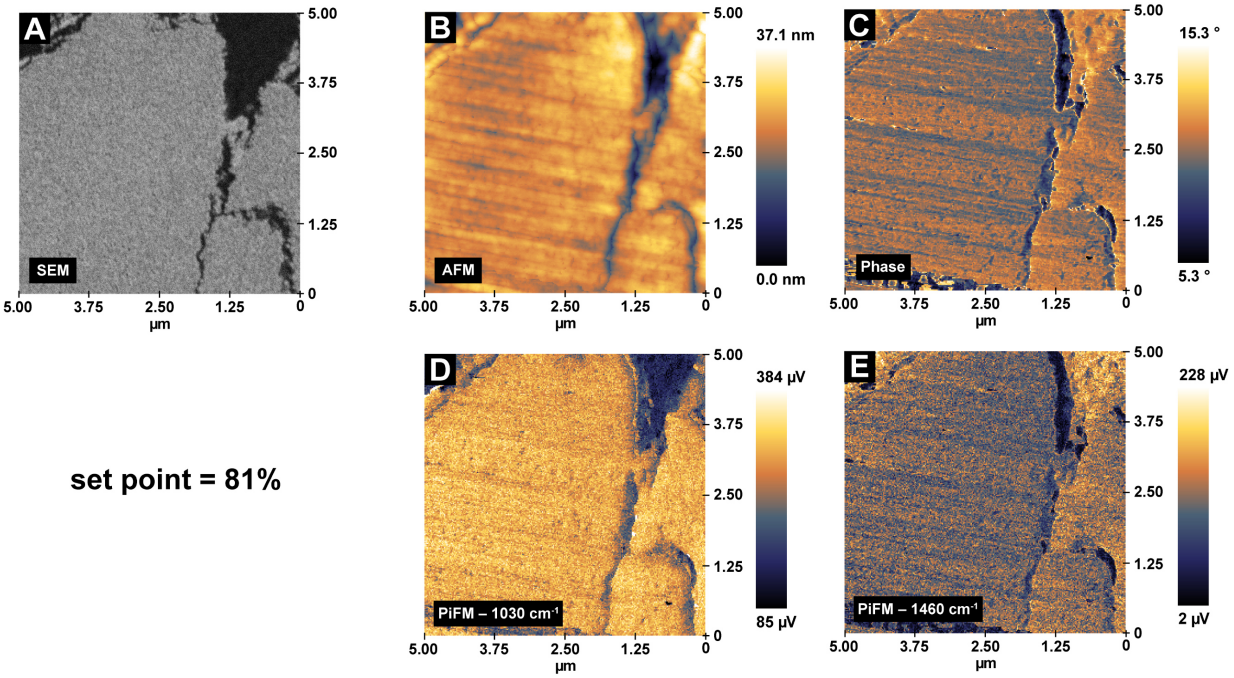

Figure S7. Scanning electron microscopy (SEM; A), topography (atomic force microscopy, AFM; B), phase shift (C) and infrared photoinduced force microscopy (IR PiFM, ν(Si–O): 1030 cm^{-1} and δ(C–H), 1460 cm^{-1}; D, E) images recorded on a single area of a 30 min pre-polymerized hafnocene-based catalyst particle cross-section (Cross-section 1, in close vicinity to measurement area shown in Figures 4C–C''', main text). The presence of a partially empty network of cracks in the silica support is discernible.

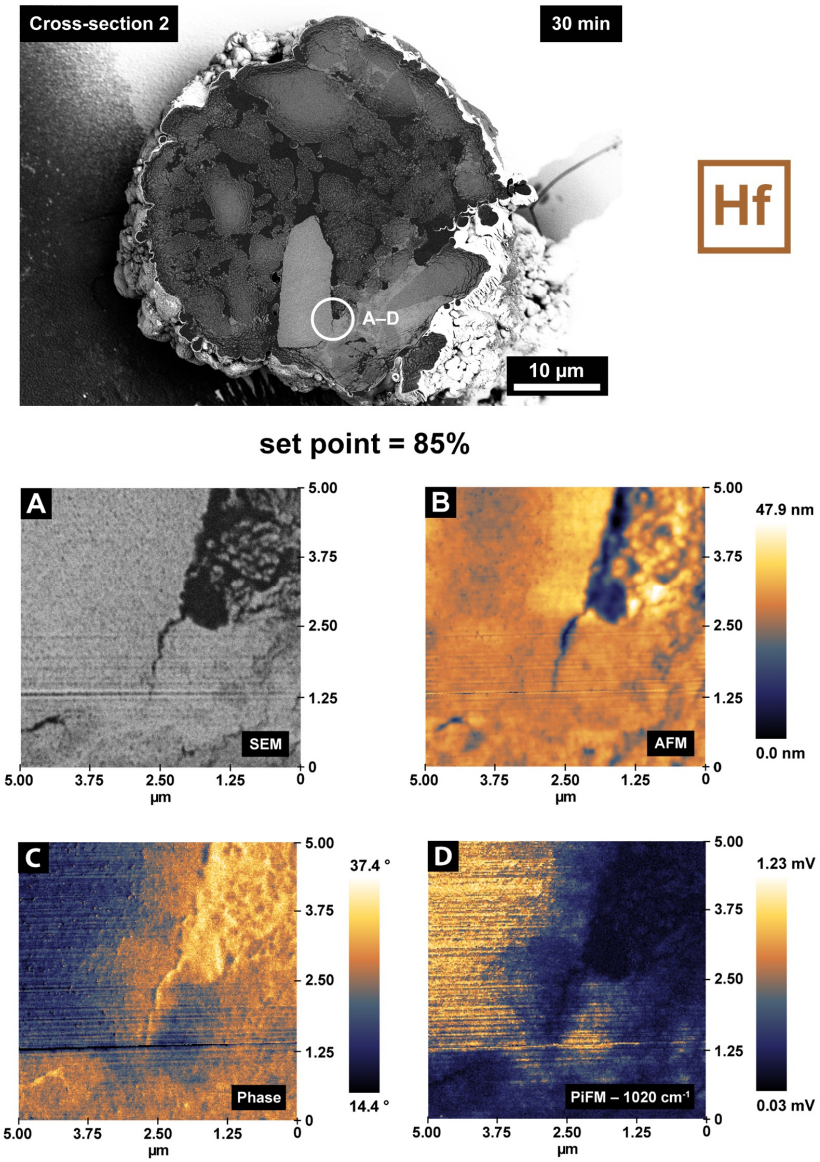

Figure S8. Scanning electron microscopy (SEM; A), topography (atomic force microscopy, AFM; B), phase shift (C) and infrared photoinduced force microscopy (IR PiFM, ν(Si–O): 1020 cm^{-1}; D) images recorded on a single area of a 30 min pre-polymerized hafnocene-based catalyst particle cross-section (Cross-section 2, Figure 2C in main text).

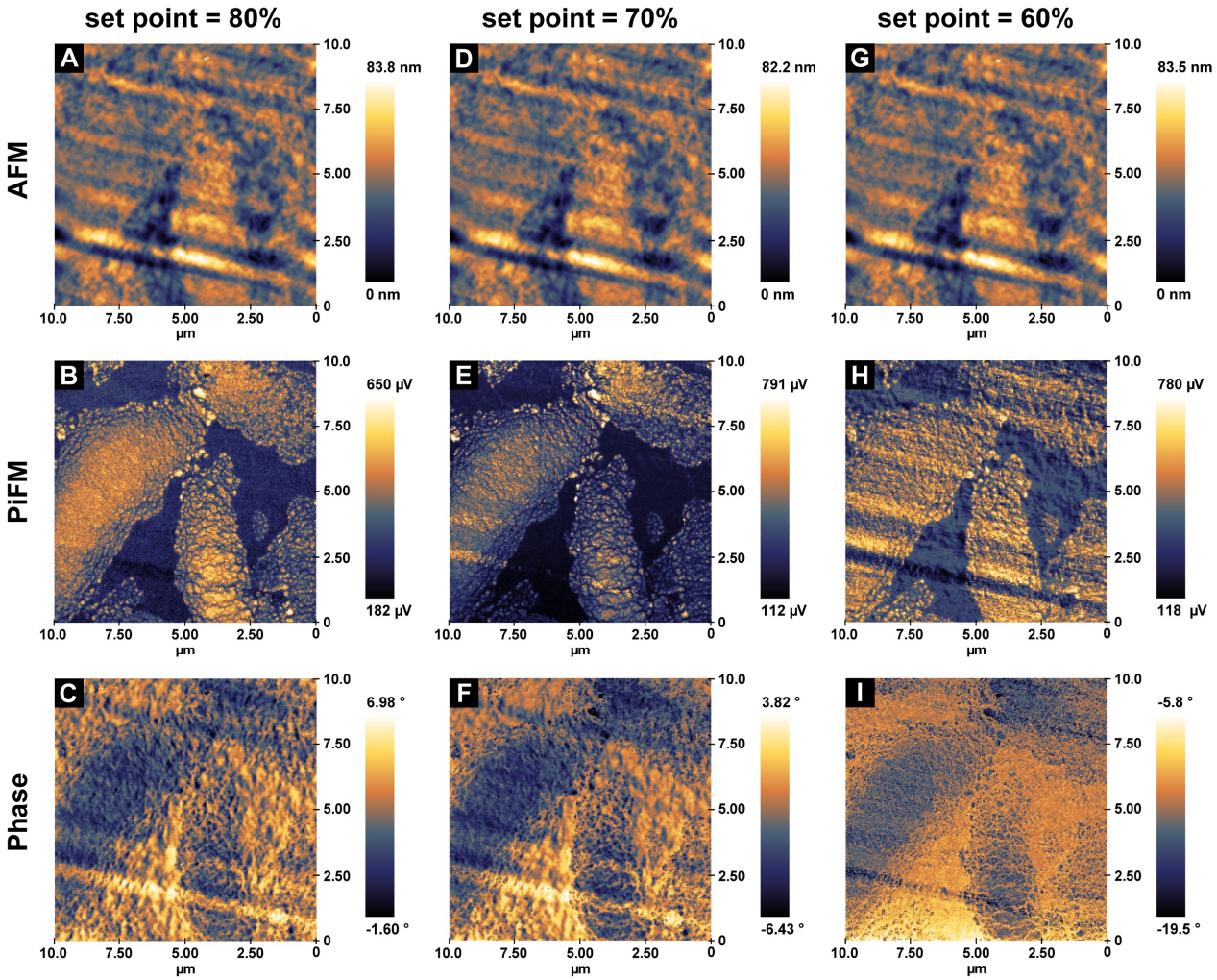

Figure S9. Topography (atomic force microscopy, AFM; A, D, G), infrared photoinduced force microscopy (IR PiFM, ν(Si–O): 1050–1030 cm^{-1}; B, E, H) and phase shift images (C, F, I) recorded on a single area of a 30 min pre-polymerized hafnocene-based catalyst particle cross-section (Cross-section 1, Figures 4A–4A'' in main text). The cantilever set point was varied to study its influence on AFM, IR PiFM and phase shift imaging. A set point of 80% was found to yield optimal IR PiFM maps. A lower set point of 60% produced better phase shift images due to the increased contact between the sample and the tip. A greater contribution of sample topography is observed in the IR PiFM images recorded at 60% set point.

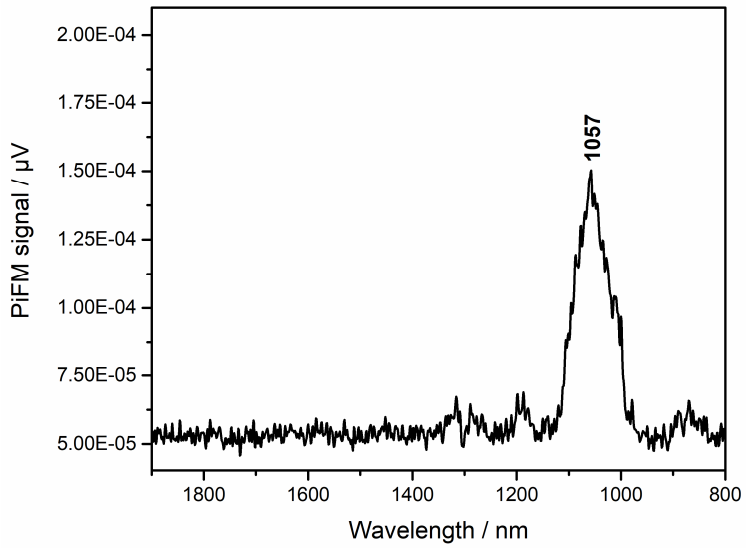

Figure S10. Infrared (IR) point spectrum recorded with infrared photoinduced force microscopy (IR PiFM) on the horizontal cross-section of a pristine hafnocene-based catalyst particle.

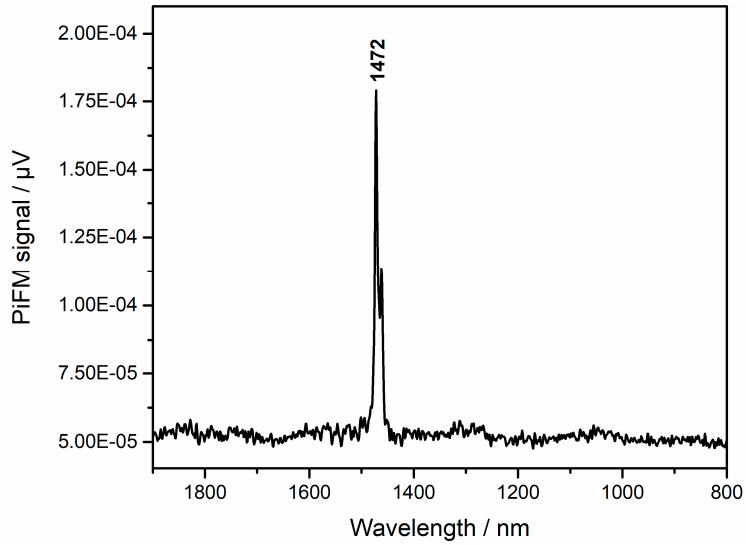

Figure S11. Infrared (IR) point spectrum recorded with infrared photoinduced force microscopy (IR PiFM) on the horizontal cross-section of a high-density polyethylene bead (Sigma-Aldrich).

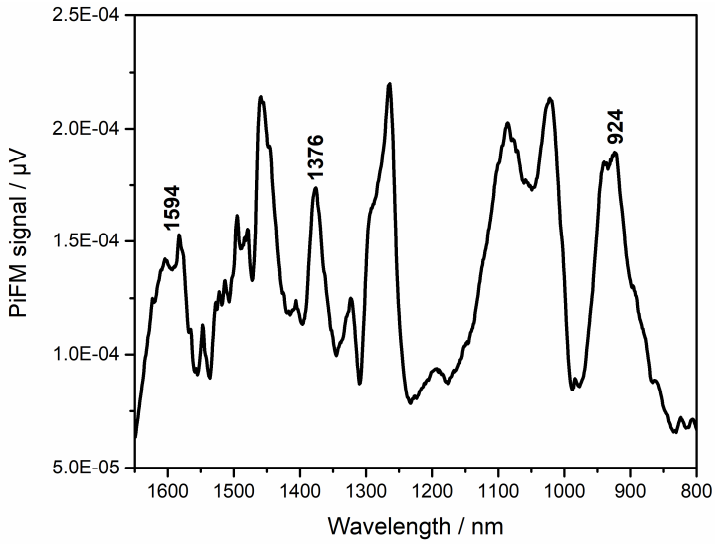

Figure S12. Infrared (IR) point spectrum recorded with infrared photoinduced force microscopy (IR PiFM) of a PE/SiO_2 composite damaged by the IR laser. A 2nd-order Savitzky–Golay filter was applied to decrease the level of background noise.

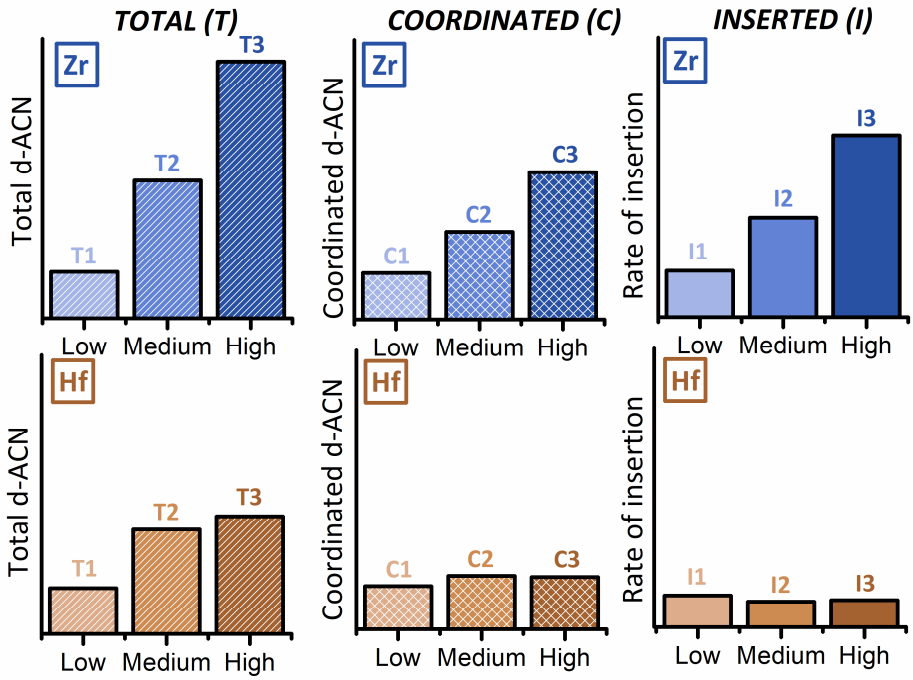

Figure S13. For each of the experiments reported in Figure 7 (main text), the maximum intensity of the FT-IR absorption bands *T* and *C* was determined by extrapolating the linear part of the curves (indicated as Tn and Cn, where n = 1, 2, 3 refers to the experiments at low, medium and high d-ACN concentration). The insertion rate was derived from the slope of the linear part of the I curves (In, with n = 1, 2 and 3).

References

(1) Meier, G. B.; Weickert, G.; Van Swaaij, W. P. M. Gas-Phase Polymerization of Propylene: Reaction Kinetics and Molecular Weight Distribution. *J. Polym. Sci. Part A Polym. Chem.* **2001**, *39* (4), 500–513.

(2) Namkajorn, M.; Alizadeh, A.; Somsook, E.; McKenna, T. F. L. Condensed-Mode Cooling for Ethylene Polymerization: The Influence of Inert Condensing Agent on the Polymerization Rate. *Macromol. Chem. Phys.* **2014**, *215* (9), 873–878.

(3) Martins, A. R.; Cancelas, A. J.; McKenna, T. F. L. A Study of the Gas Phase Polymerization of Propylene: The Impact of Catalyst Treatment, Injection Conditions and the Presence of Alkanes on Polymerization and Polymer Properties. *Macromol. React. Eng.* **2017**, *11* (1), 1600011.

(4) Bossers, K. W.; Valadian, R.; Garrevoet, J.; van Malderen, S.; Chan, R.; Friederichs, N.; Severn, J.; Wilbers, A.; Zanoni, S.; Jongkind, M. K.; et al. Heterogeneity in the Fragmentation of Ziegler Catalyst Particles during Ethylene Polymerization Quantified by X-Ray Nanotomography. *JACS Au* **2021**, *1* (6), 852–864.

(5) De Winter, D. A. M.; Meirer, F.; Weckhuysen, B. M. FIB-SEM Tomography Probes the Mesoscale Pore Space of an Individual Catalytic Cracking Particle. *ACS Catal.* **2016**, *6* (5), 3158–3167.

(6) Murdick, R. A.; Morrison, W.; Nowak, D.; Albrecht, T. R.; Jahng, J.; Park, S. Photoinduced Force Microscopy: A Technique for Hyperspectral Nanochemical Mapping. *Jpn. J. Appl. Phys.* **2017**, *56* (8).

(7) Nowak, D.; Morrison, W.; Wickramasinghe, H. K.; Jahng, J.; Potma, E.; Wan, L.; Ruiz, R.; Albrecht, T. R.; Schmidt, K.; Frommer, J.; et al. Nanoscale Chemical Imaging by Photoinduced Force Microscopy. *Sci. Adv.* **2016**, *2* (3).

(8) Carrasco, F.; Pagès, P.; Pascual, S.; Colom, X. Artificial Aging of High-Density Polyethylene by Ultraviolet Irradiation. *Eur. Polym. J.* **2001**, *37* (7), 1457–1464.

(9) Yang, T. C. K.; Lin, S. S. Y.; Chuang, T. H. Kinetic Analysis of the Thermal Oxidation of Metallocene Cyclic Olefin Copolymer (MCOC)/TiO_2 Composites by FTIR Microscopy and Thermogravimetry (TG). *Polym. Degrad. Stab.* **2002**, *78* (3), 525–532.

(10) Lazar, G.; Zellama, K.; Vascan, I.; Stamate, M.; Lazar, I.; Rusu, I. Infrared Absorption Properties of Amorphous Carbon Films. *J. Optoelectron. Adv. Mater.* **2005**, *7* (2), 647–652.

(11) Gardette, M.; Perthue, A.; Gardette, J. L.; Janecska, T.; Földes, E.; Pukánszky, B.; Therias, S. Photo- and Thermal-Oxidation of Polyethylene: Comparison of Mechanisms and Influence of Unsaturation Content. *Polym. Degrad. Stab.* **2013**, *98* (11), 2383–2390.

(12) Huth, F.; Govyadinov, A.; Amarie, S.; Nuansing, W.; Keilmann, F.; Hillenbrand, R. Nano-FTIR Absorption Spectroscopy of Molecular Fingerprints at 20 nm Spatial Resolution. *Nano Lett.* **2012**, *12* (8), 3973–3978.

(13) Bechtel, H. A.; Johnson, S. C.; Khatib, O.; Muller, E. A.; Raschke, M. B. Synchrotron Infrared Nano-Spectroscopy and -Imaging. *Surf. Sci. Rep.* **2020**, *75* (3), 100493.